3-2024

Wavelength-induced shedding frequency modulation of seal whisker inspired cylinders

Trevor Dunt
University of Wisconsin-Madison

Kirby S. Heck
University of Wisconsin-Madison

Kathleen Lyons
University of Wisconsin

Christin Murphy
University of Wisconsin-Madison

Raul Bayoan Cal
Portland State University, rcal@pdx.edu

See next page for additional authors

Citation Details

Authors

Trevor Dunt, Kirby S. Heck, Kathleen Lyons, Christin Murphy, Raul Bayoan Cal, and Jennifer A. Franck

Wavelength-induced shedding frequency modulation of seal whisker inspired cylinders

1
2
3
4
5
6
7
8
9
10
11
12
13
14
15
16
17
18
19
20
21
22
23
24
25
26
27
28
29
30
31
32
33
34
35
36
37
38
39
40
41
42
43
44
45
46
47
48
49
50
51
52
53
54
55
56
57
58
59
60

Wavelength-induced shedding frequency modulation of seal whisker inspired cylinders

T K Dunt[1]‡, **K S Heck**[1]‡, **K Lyons**[1], **C T Murphy**[2], **R B Cal**[3], **J A Franck**[4]

[1] Department of Engineering Physics, University of Wisconsin–Madison, Madison WI

[2] Naval Undersea Warfare Center - Newport, Newport RI

[3] Department of Mechanical & Materials Engineering, Portland State University, Portland OR

[4] Department of Mechanical Engineering, University of Wisconsin–Madison, Madison WI

E-mail: jafranck@wisc.edu

‡ These authors contributed equally to this work.

Shedding frequency of seal whiskers   2

Abstract

The spanwise undulated cylinder geometry inspired by seal whiskers has been shown to alter shedding frequency and reduce fluid forces significantly compared to smooth cylindrical geometry. Undulation wavelength is systematically investigated in order to explore its effect on unsteady lift force and shedding frequency. Prior research has parameterized the whisker-inspired geometry and demonstrated the relevance of geometric variations on force reduction properties. Among the geometric parameters, undulation wavelength was identified as a significant contributor to forcing changes. To analyze the effect of undulation wavelength, a thorough investigation isolating changes in wavelength is performed to expand upon previous research that parameterized whisker-inspired geometry and the relevance of geometric variations on the force reduction properties. A set of five whisker-inspired models of varying wavelength are computationally simulated at a Reynolds number of 250 and compared with an equivalent aspect ratio smooth elliptical cylinder. Above a critical non-dimensional value, the undulation wavelength reduces the amplitude and frequency of vortex shedding accompanied by a reduction in oscillating lift force. Frequency shedding is tied to the creation of wavelength-dependent vortex structures which vary across the whisker span. These vortices produce distinct shedding modes in which the frequency and phase of downstream structures interact to decrease the oscillating lift forces on the whisker model with particular effectiveness around the wavelength values typically found in nature. The culmination of the these location-based modes produces a complex and spanwise-dependent lift frequency spectra at those wavelengths exhibiting maximum force reduction. Understanding the mechanisms of unsteady force reduction and the relationship between undulation wavelength and frequency spectra is critical for the

Shedding frequency of seal whiskers　　　　　　　　　　　　　　　　　　　　　3

application of this geometry to vibration tuning and passive flow control for vortex-induced vibration (VIV) reduction.

1. Introduction

Unsteady forces and the associated shedding frequency modification of flow over seal whisker inspired undulated cylinders are investigated. Seals possess an impressive ability to follow hydrodynamic disturbances without visual or auditory stimuli [1] and even distinguish between wakes shed by different objects [2]. These abilities are partially attributed to the unique morphology of their whiskers. Unlike other mammals, seal whiskers have undulations along their span. Opposing sets of undulations run along both faces of the whisker length and can be defined by two tilted ellipses of varying aspect ratio situated one half-wavelength apart (Figure 1). A near-sinusoidal surface swept between repeating sets of these elliptical cross sections forms an undulated cylinder. As flow passes over the whisker, undulations introduce spanwise momentum transport leading to the breakup of the long, connected vortex structures typically shed by smooth cylinders [3]. A trademark of flow over cylindrical and similar bluff-bodies is the shedding of coherent, alternating-signed vortices known as a von Kármán vortex street. The alternating low pressure cores of these vortices give rise to a fluid-structure interaction called vortex-induced vibration. VIV is responsible for undesirable structural motion causing fatigue and failure in a wide variety of engineering systems [4]. Seals utilize their highly sensitive whiskers to detect flow disturbances and their origin to track prey via their hydrodynamic wake. As a bluff body flow sensor, even in calm or uniform flows, VIV can overwhelm signal data from the targeted scale of flow disturbances of interest [5]. By breaking up the cohesive vortex shedding, a seal whisker geometry reduces VIV and improves the signal-to-noise ratio when sensing disturbances in oncoming flow [5, 6].

The quantitative relationship between geometric properties and the hydrodynamic response can be shown through examination of the fluid dynamics, including the relationship between the undulation wavelength geometry and the frequency spectrum of vortex shedding. The seal whisker geometry was first parameterized by Hanke et al., who laid out nominal geometric values based on measurements of undulations on seven harbor seal whiskers [3]. Since then, several investigations have examined variations of this nominal geometry [3, 7, 8, 9, 10, 11, 12], uncovering important geometric features influencing the flow response. For example, Hans et al. discovered that the dual undulations of the whisker morphology were more efficient at reducing forces than one set of undulations in a single direction which were inadequate in weakening or breaking up shed vortices [7]. Liu et al. followed by concluding that the phase difference between the chord and thickness undulations is also critical for lift and drag reduction [8]. In an attempt to assess the relevance of individual geometric parameter modifications, Lyons et al. concluded that mean aspect ratio, undulation amplitude, and undulation wavelength were most impactful to the reduction of lift and drag forces [9]. In follow-up investigations, Yuasa et al. more thoroughly documented the unsteady hydrodynamic effects of varying undulation amplitudes [11] and Lyons et al. explored mechanisms of drag reduction as a function of wavelength utilizing a turbulent kinetic energy balance within the wake [12]. Vortex shedding by whisker-like geometries is also affected by the angle of attack of the incoming flow. In their study of whisker wavelength and angle of attack, Kim and Yoon found that non-zero angles of attack less than 30 degrees reduced but did not eliminate the effects of surface undulations. However this prior research did not include the analysis of wavelength-dependent vortex shedding frequency as relevant to fluid forces and wake structures.

Other controlled, simple geometries reminiscent of some seal whisker features have

been shown to cause similar effects as this more complex, bioinspired structure. The addition of undulated or wavy patterns to smooth geometries have been shown to create increasingly three dimensional flow as well as influence mean coefficient of drag and root mean square (RMS) lift coefficient. By adding a wavy pattern to the trailing edge of a blunt edged half-ellipse, Bearman and Tombazis saw a reduction of base drag of their model as well as concentration of forces dependent upon spanwise position along trailing edge waves [13]. Also shown were the development of distinct shedding frequencies with respect to spanwise location. This spatial dependence was responsible for the development of shedding modes defined by spanwise regions referred to as cells. Each contains isolated vortex shedding behavior from adjacent cells and, consequently, the shedding frequency in each cell results in both symmetric and antisymmetric behaviors depending on model wavelength. Lam and Lin later studied the effects of wavelength and amplitude variation for a wavy surface applied to axisymmetric cylinder with sinusoidal variations in radius [14]. They observed that their geometry formed a three-dimensional, periodic free shear layer at all wavelengths tested and also documented the appearance of optimal wavelengths resulting in the greatest reduction of mean drag and RMS lift coefficients.

The keen sensing abilities of seal whiskers are also desirable as a basis for bioinspired sensing technology. Flow sensors utilizing a harbor seal whisker geometry have been experimentally investigated and shown to identify vortex wakes generated from upstream bodies. For the design and noise mitigation of these sensors, characterizing the frequency effects of geometric variables has been an important focus of prior research. Most prominently, Beem and Triantafyllou tested two different geometries of varying undulation wavelength in a whisker-inspired sensor and found that a wavelength longer than that originally reported by Hanke et al. was more successful at suppressing

Shedding frequency of seal whiskers 6

vibrations over a wide range of flow velocities [5]. Thus, within the parametric exploration of seal whisker inspired geometries to date, undulation wavelength has been noted as a contributor to flow response changes [15], but has yet to be thoroughly investigated in terms of the underlying mechanisms leading to differences in shedding frequency.

This investigation utilizes a rigid numerical model of a whisker-inspired geometry to assess the influence of spanwise undulation wavelength on the lift frequency spectra generated from unsteady, three-dimensional vortex shedding. This is accomplished through detailed computational simulations that link the changes in the amplitude and frequency of the unsteady forces to the formation of shed vortices and wake structure as a function of wavelength position. Such models are useful in understanding how whisker inspired geometry will respond to various types of flow and in choosing the appropriate undulation topography for a specific application. The conclusions drawn between wavelength of undulation and resulting unsteady hydrodynamic performance can inform the design and improve effectiveness of bioinspired applications of seal whisker geometry for the suppression of VIV and modification of the vibration noise spectrum.

The following sections are organized into Section 2 where the whisker geometry, numerical model, and flow parameters are introduced, Section 3 in which the force response and fluid dynamics mechanisms responsible for the changes in force patterns are summarized, and Section 4 where concluding remarks are given.

Shedding frequency of seal whiskers   7

2. Methods

2.1. Undulated Cylinder Geometry

The geometric parameters of the undulated cylinder follow those introduced by Lyons et al. [9] which produces an equivalent geometry to Hanke et al. [3] except with redefined parameters that can be independently varied and non-dimensionalized with hydrodynamic significance. The schematic in Figure 1 shows the non-dimensional mean thickness T and mean chord length C which are parallel and perpendicular to the incoming flow along the positive x-direction, respectively and are related by an aspect ratio $\gamma = C/T$. Both chord length and thickness vary along the spanwise direction due to surface undulations and are a function of z, the spanwise coordinate. The amplitudes of these undulations are given by A_C and A_T and each vary at a wavelength λ with all three parameters non-dimensionalized by mean thickness T. Leading and trailing edge undulations are offset by ϵ, and trough locations are shifted by a value Φ. Due to the influence of ϵ and Φ, the spanwise profile is not perfectly sinusoidal and is instead defined by a directionally biased piecewise function.

In this research, the values of all geometric parameters remain fixed at $\gamma = 1.9$, $A_T = 0.09$, $A_C = 0.23$, $\epsilon = 0.34$, and $\phi = 0.015$ except the non-dimensional wavelength, λ, which is varied from $\lambda = 1, 2, 3.43, 5$, and 6.86. The non-dimensional wavelength of 3.43 is chosen because it is equivalent to the geometric parameterization performed by Hanke et al. [3], and has been widely investigated in literature. Thus, the nominal wavelength of $\lambda = 3.43$ is biologically relevant; however, it should be noted that there is sufficient geometric diversity within and across species [16, 17] and not all seal whiskers closely follow this model geometry. A smooth elliptical cylinder of equal aspect ratio is also simulated.
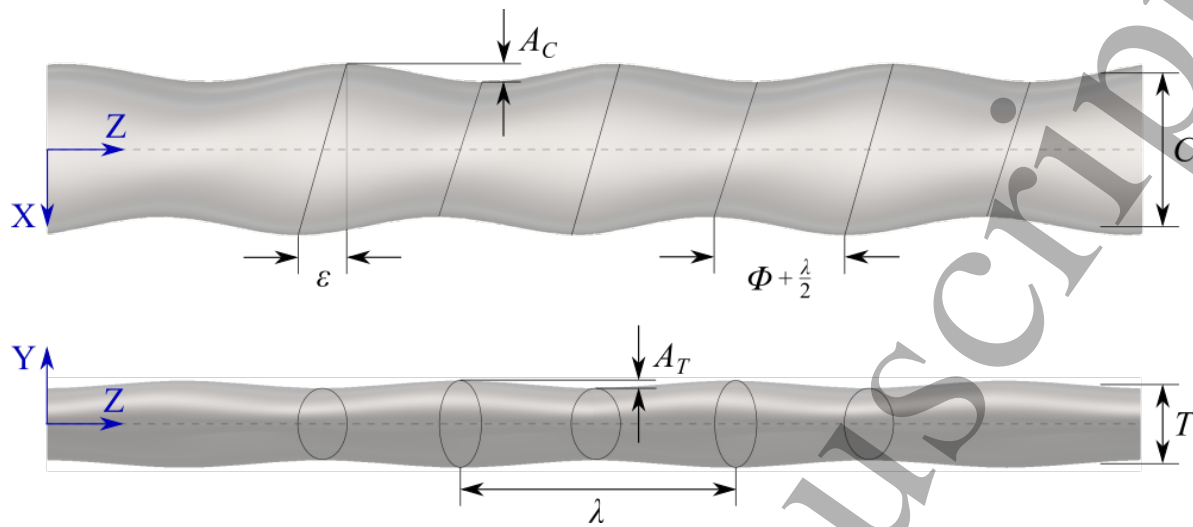
Shedding frequency of seal whiskers   8

Figure 1: Whisker geometric parameter schematic diagram.

2.2. Numerical methods

The unsteady, time-accurate simulated flow field over whisker-inspired cylinders is generated by solving the incompressible Navier-Stokes equations using second-order finite-volume libraries of the open-source numerical solver *OpenFOAM* [18] using direct numerical simulation. Numerical stability is maintained while optimizing simulation performance through the use of dynamic time stepping via the PIMPLE algorithm, a combination of pressure-implicit, split-operator (PISO) and the semi-implicit method for pressure-lined equations (SIMPLE) algorithm. The computational domain and methodology have been previously validated and presented in prior work [11, 12], but are briefly described below.

The computational domain consists of an outer cylinder with a radius of $75T$ with the whisker geometry in the center. The y-z plane splits the outer boundary into inlet and outlet conditions, no-slip conditions are enforced along the whisker surface, and periodic boundary conditions are applied along the span approximating an infinite-length whisker geometry. The model span is two wavelengths, $L_z = 2\lambda$, thus the total span L_z will change for each wavelength as listed in Table 1. Previous research

has determined that two full wavelengths are sufficient to capture the prominent flow structures in the $\lambda = 3.43$ model [19]. To confirm this is also true in the smallest wavelength models, an additional simulation of the $\lambda = 1$ model is performed with $L_z = 4\lambda$. The frequency spectra consistently displayed the same peaks as the model with $L_z = 2\lambda$.

An accurate and repeatable structured computational mesh is generated using a mesh morphing algorithm developed by Yuasa et al. [11]. Each simulation starts with a smooth cylindrical mesh of near-wall resolution $0.003T$ and 20 wall-normal nodes within the boundary layer at the mid-chord. After the cylinder flow has converged to its fully developed state the undulations of the whisker are prescribed through a mesh motion function, which maintains the structured mesh resolution throughout the domain, and assures appropriate resolution on the near surface. Across the different models, the radial, tangential and spanwise resolution is constant. As a result, the spanwise domain, L_z, and thus the total number of points in the spanwise direction, varies to accomodate the longer wavelength whiskers. Meshing numerical details are provided in Table 1.

2.3. Simulation and Flow Parameters

Flow around each whisker wavelength model was simulated at zero angle of attack (coincidence with $+x$-direction) to approximate nominal forward swimming where undulated surface effects are most dramatic. All simulations were performed at Reynolds number $Re = U_\infty T/\nu$ of 250 where U_∞ is the freestream velocity and ν is the kinematic viscosity of the fluid. Mean thickness T is chosen as a characteristic length as previously defined by Lyons et al. and Yuasa et al. [9, 11]. Other seal whisker researchers have also utilized hydraulic diameter, D_h [20] as well as mean diameter, D_m [21]. Comparison can be made to these alternate characteristic length scales by the ratio of mean thickness to hydraulic diameter, $T/D_h = 0.781$, thickness to mean diameter, $T/D_m = 0.685$, or

Shedding frequency of seal whiskers 10

$T/C = 0.521$. This Reynolds number corresponds to a swimming speed of 0.5 meters per second which is within a range of flow speeds commonly experienced by harbor seals [3, 22]. Computational probes positioned *a-priori* in the near-wake region within the shear layer of the flow ($x/T = 1.342, y/T = \pm 0.625$) sampled instantaneous velocity and pressure at an interpolated constant time step along fifteen spanwise locations at intervals of $\Delta z/T = \lambda/8$ of which three are used in later analysis for locations shown by the schematic in Figure 2.
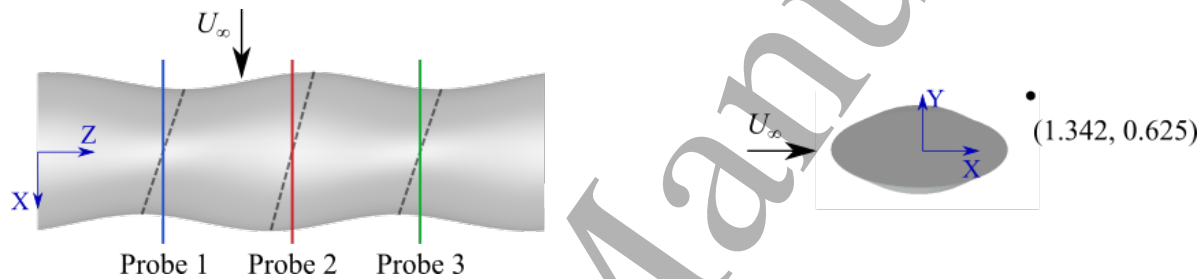

Figure 2: Top and side views defining the probe positions for sampled pressure spectra.

Time-resolved forces on the whisker body in the x and y directions are utilized to calculate coefficients of drag and lift which are non-dimensionalized by the frontal area TL_z and planform area CL_z of each wavelength model,

$$C_D(t) = \frac{2F_x(t)}{\rho U_\infty^2 TL_z} \quad \text{and} \quad C_L(t) = \frac{2F_y(t)}{\rho U_\infty^2 CL_z}. \tag{1}$$

The whisker has no camber and as a result the mean lift coefficient is nominally zero, though wavelengths $\lambda = 3.43$ and 5 demonstrate small skewed mean values that likely result from flow instabilities and not geometric asymmetry. Instead, the quantity of interest is the amplitude and frequency of lift oscillations. The amplitude is represented by the root-mean-square of the lift coefficient, or $C_{L,RMS}$. The pressure and shear stresses are also integrated over 32 equal spanwise increments generating a discrete spanwise representation of the forces, $F_x(z,t)$ and $F_y(z,t)$, and a location dependence

of the force coefficients, $C_D(z,t)$ and $C_L(z,t)$. To observe periodic trends a fast Fourier

transform (FFT) is performed on an 800 convective time unit lift coefficient series

recorded after flow is fully developed for each wavelength with a sampling rate of 0.02.

This is used to transform the time-resolved quantities into the frequency domain f,

where a reduced frequency,

$$f^* = \frac{fT}{U_\infty},\tag{2}$$

is reported using mean thickness T as a characteristic length. Utilizing the spanwise

force binning procedure and the spanwise distribution of probes described above, the

reduced frequency can also be a function of span (z) or a result of the span-averaged

lift force signal. For this application, in terms of analyzing frequency of oscillations in

the lift force spectra, the Strouhal number, St, denotes the reduced frequency with the

highest amplitude.

Finally, to visualize the vortex structures that give rise to the oscillating forces,

isosurfaces of Q-criteria are displayed, where $Q = \frac{1}{2}[||\Omega_{ij}||^2 - ||S_{ij}||^2]$ and Ω_{ij} is the

velocity rotation rate tensor and S_{ij} is the rate of strain tensor. Positive Q-criterion

denotes regions where the rotation of the flow dominates over elongation of the flow and

is associated with vortex structure [23].

Table 1: Geometry mesh size and resolution parameters of modified whisker models.

	L_z/T	$\Delta z/T$	N_z	N_θ	N_r	N_{total}
Ellipse	6.86	0.041	170	160	154	4.14M
$\lambda = 1$	2	0.041	50	160	154	1.20M
$\lambda = 2$	4	0.041	100	160	154	2.42M
$\lambda = 3.43$	6.86	0.041	170	160	154	4.14M
$\lambda = 5$	10	0.041	248	160	154	6.05M
$\lambda = 6.86$	13.73	0.041	340	160	154	8.30M

Shedding frequency of seal whiskers
12

3. Results

In this section the effects of wavelength changes on unsteady forces and the structures and fluid behavior are investigated.

3.1. Shedding Frequency Dependence on Wavelength

All whisker models investigated show a reduction in amplitude of unsteady forces between wavelengths of 1 to 6.86 compared with a smooth elliptical cylinder. Since aspect ratio is an important factor in influencing the amplitude of lift oscillations [9] the smooth elliptical cylinder of equivalent mean aspect ratio is chosen as the baseline comparison rather than a circular cylinder. The RMS lift coefficient is plotted against the non-dimensional wavelength, in Figure 3. Notably, the shortest-wavelength undulations of $\lambda = 1$ have a minimal effect on the magnitude of the unsteady lift coefficient with a reduction of only 2.2% with respect to the elliptical cylinder. Fluctuating lift forces then decrease with increasing λ, and reach a minimum $C_{L,RMS} = 0.02$ at $\lambda = 3.43$ which is an order-of-magnitude decrease in unsteady forcing as compared to the elliptical cylinder. Literature for this wavelength provides rich data and the RMS lift values obtained at $\lambda = 3.43$ are in strong agreement with prior investigations [3].

Above the nominal wavelength of $\lambda = 3.43$, lift forces continue to be suppressed by an order-of-magnitude compared to the elliptical cylinder, up to the maximum wavelength tested at $\lambda = 6.86$. Although not shown, mean drag forces also decrease significantly at $\lambda > 3$, with more details provided in Lyons et al [12]. The focus of this analysis is in the frequency and amplitude of the unsteady lift forces that would drive the VIV of the cylinder. The strongest frequency in the lift coefficient spectra is extracted as a Strouhal number, shown in Figure 3 as a function of λ. This reveals

*Shedding frequency of seal whiskers*13

two distinct regimes with respect to wavelength. Coupled with similar trends in lift

forces, this split between wavelengths of $\lambda \leq 2$ and $\lambda \geq 3.43$ indicates a fundamentally

different shedding behavior as Strouhal number varies by 4% or less within these separate

wavelength groups but drops by 23% between these values due to mechanisms explored
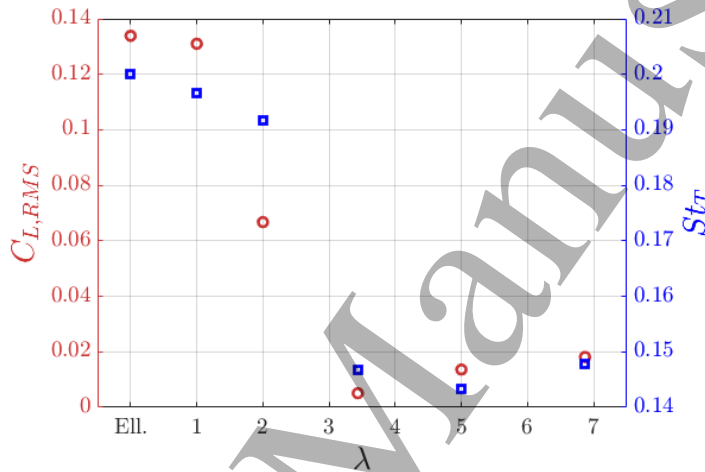
in following sections.

Figure 3: There is an order-of-magnitude decrease in unsteady lift forces in the vicinity of (and above) a nominal seal whisker wavelength $\lambda = 3.43$ relative to the 2-D elliptical cylinder. Simultaneously, the shedding frequency as categorized by the Strouhal number shows two regions, one of canonical vortex shedding for $\lambda \leq 2$ and a region of suppressed vortex shedding $\lambda \geq 3.43$.

The Strouhal number categorizes the entire spectrum of hydrodynamic forcing into

a single frequency, which for two-dimensional cylinders can often sufficiently capture

the dominant flow structures governing periodic vortex shedding. In contrast, cylinders

with spanwise variation create fully three-dimensional wake structures that are not well

categorized by a single Strouhal number or dominant vortex shedding frequency. Thus,

the full lift spectra are displayed in Figure 4, and directly compared to a smooth ellipse

at the same Reynolds number (gray line).

The peaks in the lift spectra of the short wavelength models ($\lambda \leq 2$) are all within

reduced frequency values of $f^* = 0.195 - 0.200$, and are close in frequency and amplitude
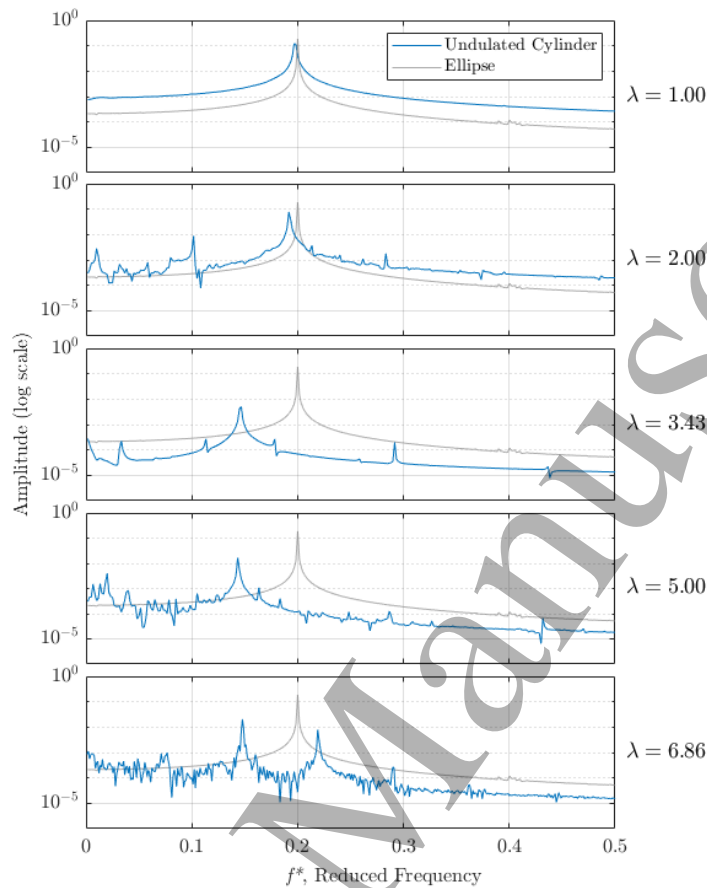
Figure 4: Spectra of unsteady lift forcing for varying wavelength with baseline ellipse geometry underlaid in gray. Spectra are normalized by the number of samples and result in non-dimensional amplitude spectral density units of C_L/f^*.

to the smooth ellipse. Higher wavelengths of $\lambda \geq 3.43$ have peaks at lower frequencies, $f^* = 0.147$ for $\lambda = 3.43$, $f^* = 0.145$ for $\lambda = 5.00$, and $f^* = 0.151$ for $\lambda = 6.86$, but solely reporting the Strouhal number obscures a secondary peak frequency for the longest wavelength model at $\lambda = 6.86$ in the lift spectrum near $f^* = 0.22$.

The bimodality in the $\lambda = 6.86$ lift spectrum is highlighted by examining local downstream pressure coefficient defined as $C_p = \frac{p - p_\infty}{\frac{1}{2}\rho U_\infty^2}$ where p is the probe pressure and p_∞ is the freestream pressure. Pressure coefficient spectra is recorded in the shear layer of the whisker model at probe positions defined in Figure 2. The pressure spectra in the wake of a whisker chord peak and trough locations as defined by Figure 5 have

Shedding frequency of seal whiskers   15

(a) $\lambda = 2$

(b) $\lambda = 3.43$

(c) $\lambda = 5$
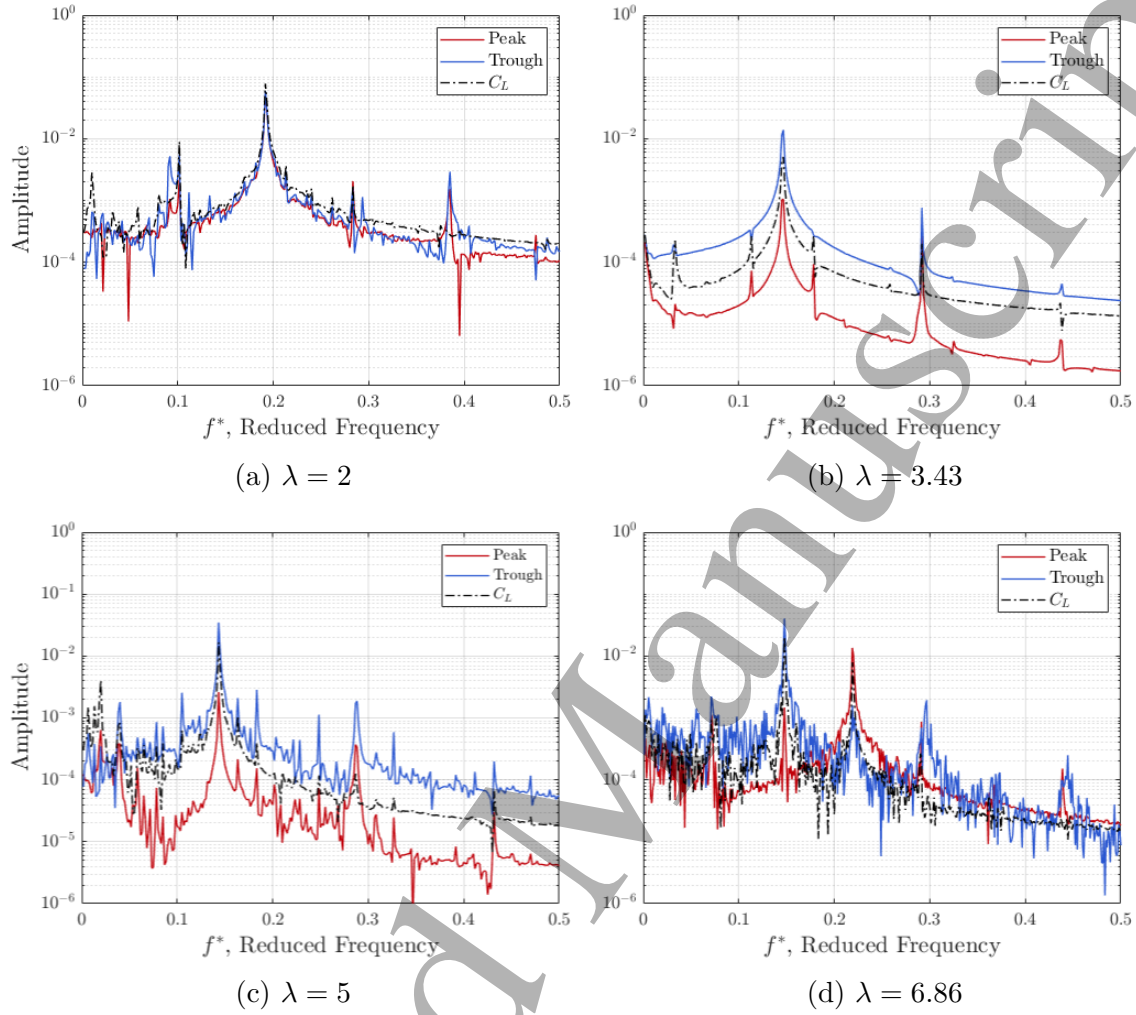
(d) $\lambda = 6.86$

Figure 5: Spectra of pressure fields at the leading-edge trough and peak spanwise locations (Probe 1 and Probe 2, respectively), non-dimensionalized to thickness T, for different undulation wavelengths. Amplitude spectral density units based on non-dimensional pressure coefficient are C_p/f^*.

one distinct peak for all whisker models which coincide with their unsteady lift signal presented in Figure 4. However, in the highest wavelength model, different spanwise locations show distinct peak shedding frequencies of $f^* = 0.151$ in trough regions and $f^* = 0.22$ for geometric peak regions which constitute both peaks observed in Figure 4.

While Figure 5 demonstrates the presence of spatially dependent shedding frequency as a function of wavelength, it does not display information about vortex shedding phase, computed as the argument of the complex Fourier coefficients. For

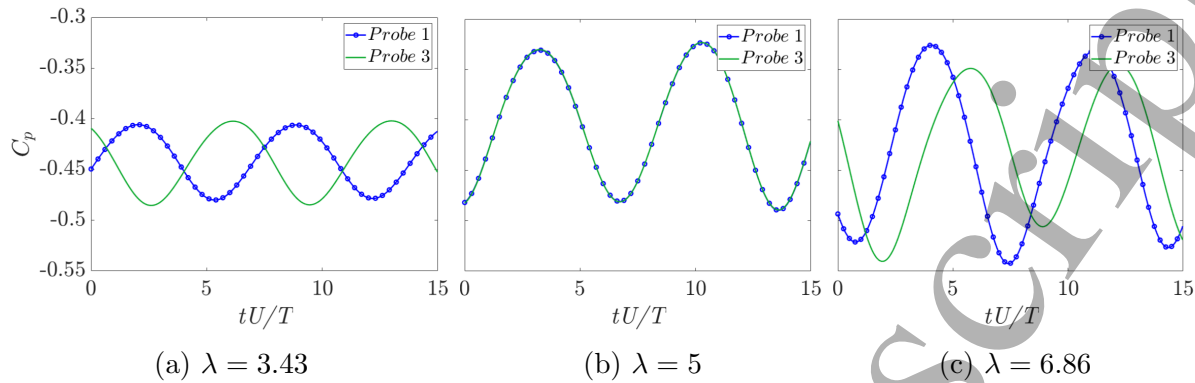(a) $\lambda = 3.43$ (b) $\lambda = 5$ (c) $\lambda = 6.86$

Figure 6: Time-resolved pressure coefficient C_p from probe points in the center wake of adjacent undulation periods for three wavelength values.

wavelengths of $\lambda \leq 2$, the phase angle of the vortex shedding is constant across the z-axis location. However, as shown in the pressure probe data in Figure 6, there is a spanwise variation in the phase angle with respect to z-location corresponding to the timing of vortex shedding for larger wavelength models. For $\lambda = 3.43$, the phase angle between two consective trough probes is approximately $180°$. This indicates that the vortex structures are alternating, or have a two-wavelength periodic pattern. In contrast at $\lambda = 5$, there is no phase difference. At the largest values $\lambda = 6.86$, there is a small but non-zero phase difference between consecutive geometry trough probes. The presence of shedding phase differences motivates a closer look at three-dimensionality in the flow to understand the implications of these frequency and phase variations on resulting fluid forces.

3.2. Three-dimensional Vortex Wake Structure

Due to the surface undulations, the whisker geometry has a cross section that varies significantly with respect to spanwise location. This spatial variation has important implications in the total force and shedding frequency of the whisker model. Figure 7 compares the fluctuating lift coefficient, normalized by the RMS value, for three

Shedding frequency of seal whiskers   17

wavelength models. The spanwise position for each model is defined on the horizontal axis and convective time on the vertical axis. The color limits and gradients between plots highlight the variation of forces with respect to time and spanwise location relative to the time-averaged RMS lift coefficient. Although not shown, the ellipse model and wavelengths $\lambda = 1$ and 2 display oscillations of nearly constant magnitude across their span contributing to larger oscillating forces. In contrast, wavelength $\lambda = 3.43$ and above demonstrate variation across the span. While these three models experienced similar reduction in magnitude of forces, the shedding pattern with respect to spanwise location has a non-uniform progression with increasing wavelength.

Borrowing terminology from Bearman & Tombazis who made similar observations using their wavy model [24], the shedding behavior seen at these wavelength values can be described in terms of similar cell-based modes but which evolve differently with trends in wavelength from their study of trailing edge undulations. Wavelength $\lambda = 3.43$ demonstrates a two-cell antisymmetric shedding mode across two undulation wavelengths. Here, two distinct vortical structures shed with equal frequency but from opposite sides while separated in span which represents a marked departure from the fully-connected structures of the smaller wavelengths and smooth geometries. For $\lambda = 5$ these structures are instead shed in tandem while still dislocated about the center similar to a two-cell symmetric mode. Finally, $\lambda = 6.86$ demonstrates a three-cell antisymmetric shedding mode with alternating regions of differing shedding frequency. Higher frequency shedding aligns with undulation peaks in the chord direction, while lower frequency oscillations occur in the trough regions. At regular intervals, these distinct shedding frequencies appear in-phase where they represent span-symmetric roller type vortices, or out of phase showing an alternating shedding behavior similar to the $\lambda = 3.43$ case.
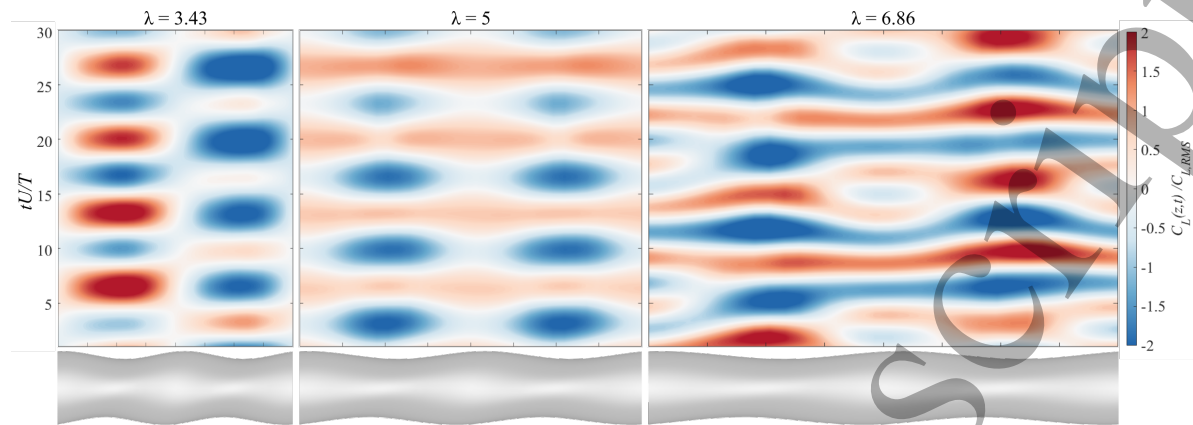
Shedding frequency of seal whiskers 18

Figure 7: Spatiotemporal plots of normalized lift coefficient for 30 simulation time units for wavelengths of $\lambda = 3.43$, 5, and 6.86 scaled horizontally by geometry length.

Next, the mechanism responsible for these forces is investigated by examining isosurfaces of Q-criterion at $Q = 0.5$. The observed phase difference in peak shedding frequencies manifests here by the timing of vortex formation. Closely mirroring results of prior literature, small wavelength models $\lambda = 1$ and $\lambda = 2$ (not shown) demonstrate little difference in shedding pattern with respect to spanwise location as consecutive undulations shed in tandem, primarily producing long, connected "roller" type vortices reminiscent of the canonical vortex streets found trailing circular or elliptical cylinders at low Reynolds numbers [9]. For wavelength $\lambda = 3.43$, "horseshoe" vortices from the top and bottom of the whisker in an alternating pattern along the span and are out of phase by nearly 180° between peak and trough locations [9, 3]. As a result of this phase difference, pressure oscillations responsible for peak shedding frequencies occur in opposite directions at approximately the same time as the low-pressure centers of vortices act on the surface. This indicates that beyond a critical wavelength value, sufficient spanwise transport is induced to cause an apparent dislocation of vortex structures with respect to each undulation period. This effect is shown from a top-down perspective in the top row of Figure 8 for a full period of vortex shedding. This phenomenon leads to a breakup of the previously observed long, connected vortex street

Shedding frequency of seal whiskers   19

shedding pattern which has been observed in literature. These structures also correlate directly with patterns in previous plots of spanwise forcing behavior shown in Figure 7.

Wavelength $\lambda = 5$ shows similarly dislocated vortices about the trailing edge geometric peak. However, vortex shedding periods with respect to space, though divided along the span, are now aligned in phase. At the largest wavelength $\lambda = 6.86$, tandem and alternating shedding patterns are both present as a function of the multiple spanwise shedding frequencies present at this wavelength. The final row of Figure 8 shows one full period of the dominant shedding frequency following the trailing edge trough regions which are separated by regions of a higher shedding frequency corresponding to the secondary peak shown in Figure 4. The interaction of these two shedding regions is also evident in a small tertiary peak frequency equal to the sum of the two previous peaks.

Evidence suggests that the alternating spanwise shedding behavior is not the primary cause of reduced force magnitude for drag and root mean square lift. Instead, the shedding frequency behavior is one aspect of an ensemble of effects contributing to the observed change in forces and shedding frequency. A more likely mechanism for the largest reduction of forces is the formation of horseshoe vortices and the modification of the magnitude and location of turbulent kinetic energy production and dissipation as recently investigated by Lyons et al. [12].

4. Conclusions

In this work, flow around five bioinspired undulated cylinder geometries, varying only in wavelength, is analyzed through measuring unsteady forces, computing lift and pressure spectra, and identifying vortex patterns from direct numerical simulation data. Of the wavelengths simulated, lift forces reach a minimum at $\lambda = 3.43$, and remain suppressed as wavelength increases up to $\lambda = 6.86$. The RMS lift fluctuations are 96.2% lower than
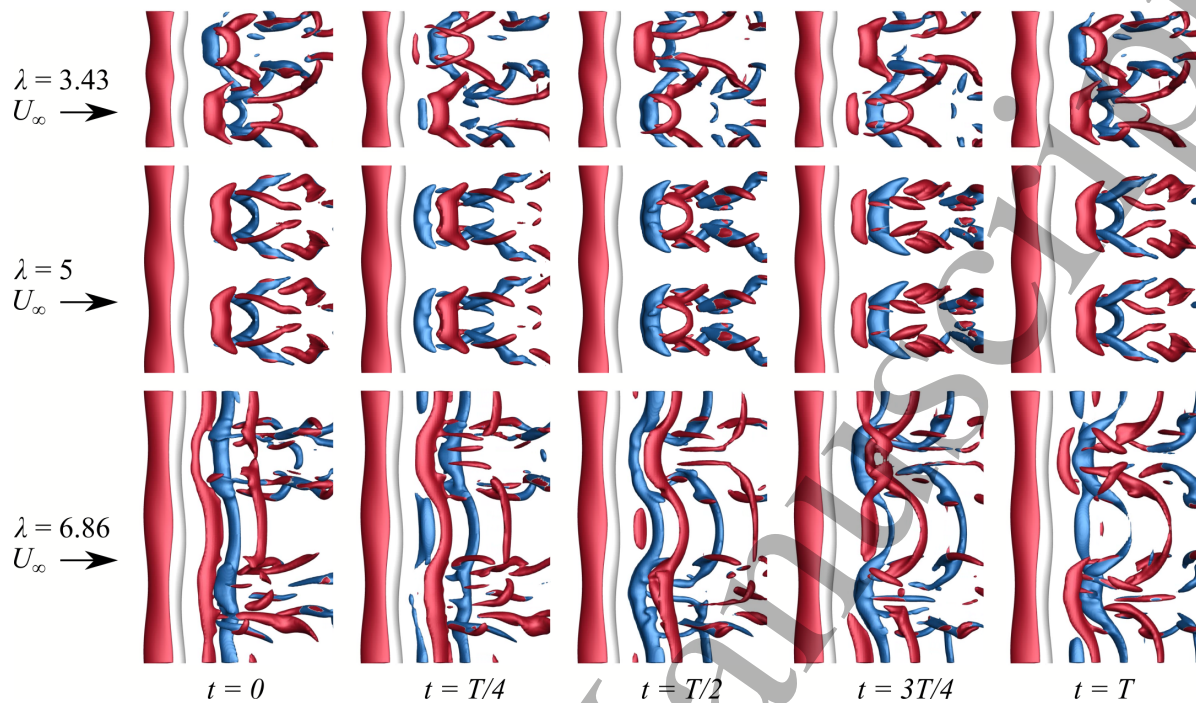
Figure 8: One period (T) of vortex shedding for wavelengths $\lambda = 3.43, 5$, and 6.86 case at low Reynolds number plotted by isosurfaces of Q-criterion at $Q = 0.5$. Red and blue coloring represent positive and negative z-vorticity, respectively.

the smooth ellipse of the same aspect ratio, and 92.4% lower than undulations with wavelength of $\lambda = 2$. In addition to lower amplitudes, the peak shedding frequency is reduced between the $\lambda = 2$ and $\lambda = 3.43$ models. Wavelengths $\lambda = 3.43$ and $\lambda = 5$ both demonstrate similar clear St peaks between $f^* = 0.145$ and 0.151. At $\lambda = 6.86$, the increasingly gentle curvature of the lengthened undulations gives rise to second peak at a higher frequency of $f^* = 0.22$.

Changes in reduced frequency are accompanied by changes in vortex shedding patterns. Wavelengths $\lambda = 2$ and lower demonstrate constant phase as a function of spanwise location typical of two-dimensional vortex shedding on a smooth cylinder. Wavelengths $\lambda \geq 3.43$ are highly three-dimensional and exhibit different modes of vortex shedding that are prevalent in the unsteady force and pressure data. At $\lambda = 3.43$, vortices form a two-cell antisymmetric mode. In this pattern, single disconnected horseshoe vortices are shed in an alternating pattern across the span, which is visualized

Shedding frequency of seal whiskers   21

by isosurfaces of Q-criterion and demonstrated by pressure probes in the wake. For wavelength $\lambda = 5$, the structure of shed vortices is similar to that of $\lambda = 3.43$, however adjacent wavelengths shed vortices in tandem, forming a two-cell symmetric shedding mode. The longest wavelength model of $\lambda = 6.86$ demonstrates a three-cell antisymmetric mode with shedding in distinct cell regions comprising of both primary shedding frequencies observed for this geometry. Pressure probes at adjacent wavelengths demonstrate a small phase angle difference, and the interaction of the two shedding frequencies is visible in the intracycle variation in spanwise forces and isosurfaces of Q-criterion.

Despite the variety of vortex shedding modes for $\lambda \geq 3.43$ wavelengths, all are accompanied by a strong suppression of fluctuating lift forces, with a decreased between 86-96% compared to a smooth ellipse. The observed effects of undulation wavelength provide both perspective on the mechanism of force reduction using this geometry as well as insights on how shedding frequency can be altered and managed through controlling wavelength. The presence of multiple shedding patterns and phase variation within the longer wavelengths where oscillating force suppression is present suggests that the primary means of reducing unsteady forces does not result from alternating shedding pattern effects but does accompany them in ensemble with other important factors. As a practical consideration for the field of bioinspired passive flow control and VIV reduction using whisker-inspired geometry, characterization of wavelength-induced shedding frequency may influence design and act as a basis for future study including fluid structure interaction or optimization of wavelength for particular applications.

Shedding frequency of seal whiskers 22

Appendix A. Reynolds Number Effects

The frequency and amplitude of lift oscillations are dependent on flow conditions, including Reynolds number. However, the overall trends in the reduction of forces and influence of shedding frequency are shown to persist for these specific wavelength models at $Re = 500$. While increasing Reynolds number results in more turbulent flow behavior, root mean square lift coefficient and reduced frequency behave similarly in this regime showing an order of magnitude decrease in lift forces. Conversely, at this Reynolds number there is an upward shift in shedding frequency as wavelength increase beyond $\lambda = 3.43$.

Accompanying the modification to peak f^*, the entire frequency spectrum for all wavelengths undergo changes at higher Reynolds number. An anticipated increase in mixing for this regime results in less coherent peaks for all wavelengths as shown in Figure A1. The most significant change occurs for $\lambda = 3.43$ where the entire spectrum shows a radically different structure. At this wavelength, low-frequency noise disrupts the periodic vortex shedding and produces a near-monotonically decreasing spectrum with only a faint peak near $f^* = 0.18$. At the two largest wavelengths, noticeable peak
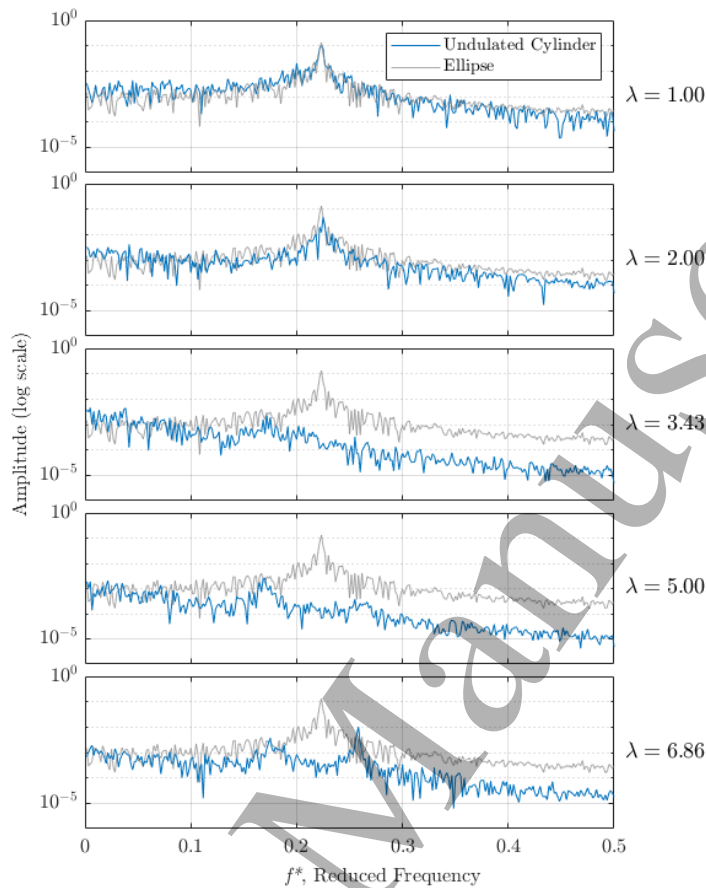
Figure A1: Spectrum of unsteady lift forcing for wavelengths for cases at $Re = 500$ with baseline ellipse geometry underlaid in gray. The frequency spectra for all wavelengths undergo some manner of shift at higher Reynolds number, though $\lambda = 3.43$ experiences the greatest change. Here, periodic vortex shedding is eschewed in favor of low-frequency noise with a near-monotonically decreasing spectrum.

frequencies appear once more and the two peaks observed for $\lambda = 6.86$ are attributed to bimodality in shedding with respect to spanwise location remain.

In the longest undulation wavelength simulated, the three-dimensional alternating vortices are still present but suppressed while the two-dimensional tandem vortices are not. This tandem mode overtakes the first shedding mode for the peak frequency. Beyond the scope of this paper, the flow response at order of magnitude larger Reynolds number regimes remains an open question with important implications for the behavior of flow sensors in conditions other than those ideal for actual seal whiskers.

Shedding frequency of seal whiskers 24

References

[1] G. Dehnhardt, B. Mauck, W. Hanke, and H. Bleckmann. Hydrodynamic trail-following in harbor seals (*Phoca vitulina*). *Science*, 293(5527):102–104, 2001.

[2] S. Wieskotten, B. Mauck, L. Miersch, G. Dehnhardt, and W. Hanke. Hydrodynamic discrimination of wakes caused by objects of different size or shape in a harbour seal (*Phoca vitulina*). *Journal of Experimental Biology*, 214(11):1922–1930, June 2011.

[3] W. Hanke, M. Witte, L. Miersch, M. Brede, J. Oeffner, M. Michael, F.D. Hanke, A. Leder, and G. Dehnhardt. Harbor seal vibrissa morphology suppresses vortex-induced vibrations. *Journal of Experimental Biology*, 213(15):2665–2672, August 2010.

[4] X. Wu, F. Ge, and Y. Hong. A review of recent studies on vortex-induced vibrations of long slender cylinders. *Journal of Fluids and Structures*, 28:292–308.

[5] H.R. Beem and M.S. Triantafyllou. Wake-induced 'slaloming' response explains exquisite sensitivity of seal whisker-like sensors. *Journal of Fluid Mechanics*, 783:306–322, November 2015.

[6] L. Miersch, W. Hanke, S. Wieskotten, F.D. Hanke, J. Oeffner, A. Leder, M. Brede, M. Witte, and G. Dehnhardt. Flow sensing by pinniped whiskers. *Philosophical Transactions: Biological Sciences*, 366(1581):3077–3084, 2011.

[7] H. Hans, J. Miao, G. Weymouth, and M.S. Triantafyllou. Whisker-like geometries and their force reduction properties. In *2013 MTS/IEEE OCEANS - Bergen, Norway*, pages 1–7, 2013.

[8] G. Liu, Q. Xue, and X. Zheng. Phase-difference on seal whisker surface induces hairpin vortices in the wake to suppress force oscillation. *Bioinspiration & Biomimetics*, 14(6), September 2019.

[9] K. Lyons, C.T. Murphy, and J.A. Franck. Flow over seal whiskers: Importance of geometric features for force and frequency response. *PLOS ONE*, 15(10):e0241142, October 2020. Publisher: Public Library of Science.

[10] K. Lyons. Effects of topography variation on fluid flow over seal whisker inspired geometries.

[11] M. Yuasa, K. Lyons, and J.A. Franck. Simulations of flow over a bio-inspired undulated cylinder with dynamically morphing topography. *Journal of Fluids and Structures*, 111:103567.

[12] K. Lyons, R.B. Cal, and J.A. Franck. Effects of wavelength on vortex structure and turbulence kinetic energy transfer of flow over undulated cylinders.

[13] N. Tombazis and P.W. Bearman. A study of three-dimensional aspects of vortex shedding from abluff body with a mild geometric disturbance. *Journal of Fluid Mechanics*, 330:85–112.

Shedding frequency of seal whiskers 25

[14] K. Lam and Y.F. Lin. Effects of wavelength and amplitude of a wavy cylinder in cross-flow at low Reynolds numbers. *Journal of Fluid Mechanics*, 620:195–220, February 2009.

[15] C.T. Murphy, W.N. Martin, J.A. Franck, and J.M. Lapseritis. *The Other Navy Seals: Seal Whiskers as a Bio-inspired Model for the Reduction of Vortex-Induced Vibrations*. Springer, June 2021.

[16] C.C. Ginter, F.E. Fish, and C.D. Marshall. Morphological analysis of the bumpy profile of phocid vibrissae. *Marine Mammal Science*, 26(3):733–743, 2010.

[17] A. Rinehart, V. Shyam, and W. Zhang. Characterization of seal whisker morphology: implications for whisker-inspired flow control applications. *Bioinspiration & Biomimetics*, 12(6), 2017.

[18] H.G. Weller, G. Tabor, H. Jasak, and C. Fureby. A tensorial approach to computational continuum mechanics using object-oriented techniques. *Computers in Physics*, 12(6):620–631, November 1998.

[19] H. Kim and H. Yoon. Effect of the orientation of the harbor seal vibrissa based biomimetic cylinder on hydrodynamic forces and vortex induced frequency. *AIP Advances*, 7(10), October 2017.

[20] M. Witte, W. Hanke, S. Wieskotten, L. Miersch, M. Brede, G. Dehnhardt, and A. Leder. On the Wake Flow Dynamics behind Harbor Seal Vibrissae – A Fluid Mechanical Explanation for an Extraordinary Capability. In Cameron Tropea and Horst Bleckmann, editors, *Results of the DFG Priority Programme 1207 "Nature-inspired Fluid Mechanics" 2006-2012*, pages 271–289. Springer, Berlin, Heidelberg, 2012.

[21] A.M. Kamat, X. Zheng, J. Bos, M. Cao, M.S. Triantafyllou, and A.G.P. Kottapalli. Undulating seal whiskers evolved optimal wavelength-to-diameter ratio for efficient reduction in vortex-induced vibrations. *Adv. Sci.*, 2023.

[22] V. Lesage, M.O. Hammill, and K.M. Kovacs. Functional classification of harbor seal (phoca vitulina) dives using depth profiles, swimming velocity, and an index of foraging success. *Canadian Journal of Zoology*, 77, 1999.

[23] J.C.R. Hunt, A.A. Wray, and P. Moin. Eddies, streams, and convergence zones in turbulent flows. In *Studying Turbulence Using Numerical Simulation Databases, 2. Proceedings of the 1988 Summer Program*, 1988.

[24] P.W. Bearman and J.C. Owen. Reduction of bluff-body drag and suppression of vortex shedding by the introduction of wavy separation lines. *Journal of Fluids and Structures*, 12(1):123–130.